Supplementary information for: Evolution of sub-ice-shelf channels reveals changes in ocean-driven melt in West Antarctica

Karen E. Alley, Richard B. Alley, Alex D. Crawford, Naomi Ochwat, Christian T. Wild, Juliana Marson, Tasha Snow, Atsuhiro Muto, Erin C. Pettit, Sarah Child, Martin Truffer, Gabi Collao-Barrios, Ted Scambos

Contents:

Figure 1a: Digitizations of channels

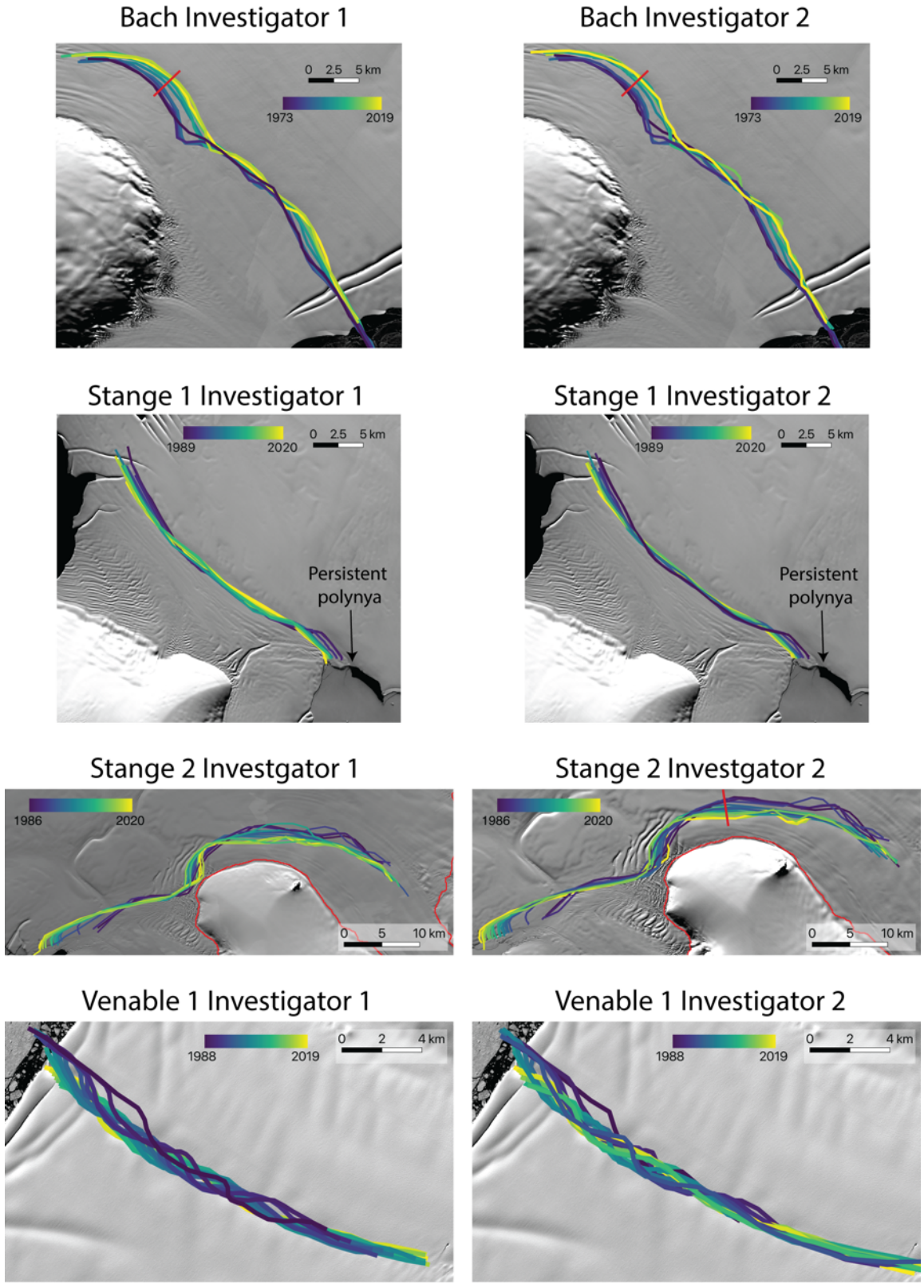

Figure 1b: Digitizations of channels continued

Venable 2 Investigator 1

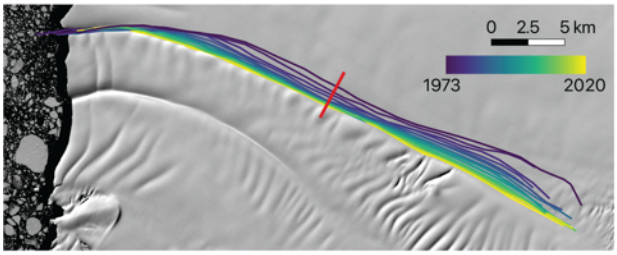

Venable 2 Investigator 2

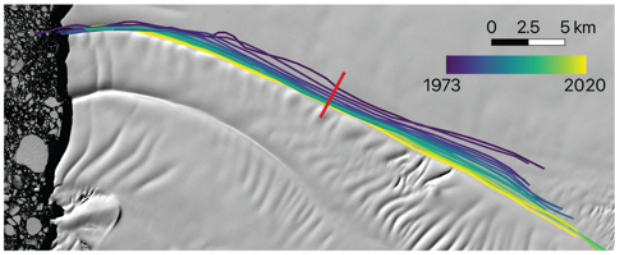

Venable 3 Investigator 1

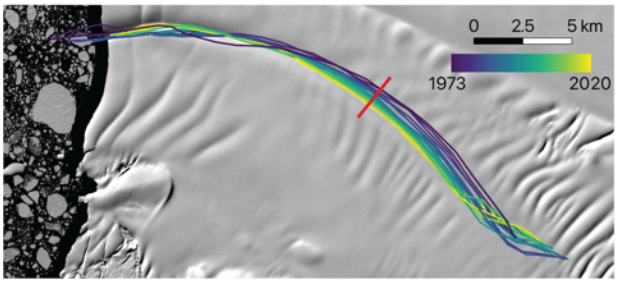

Venable 3 Investigator 2

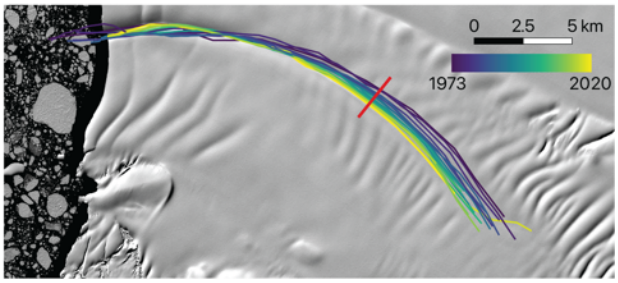

Abbot Investigator 1

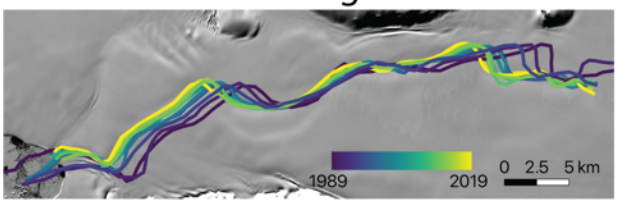

Abbot Investigator 2

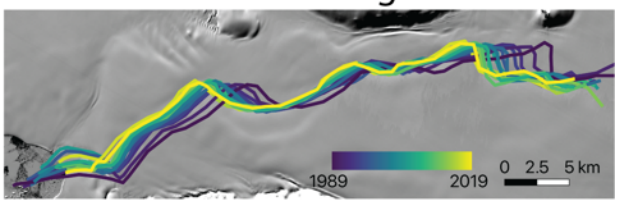

Cosgrove Investigator 1

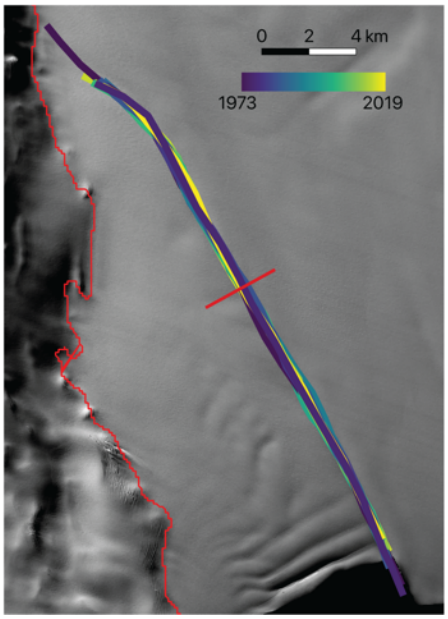

Cosgrove Investigator 2

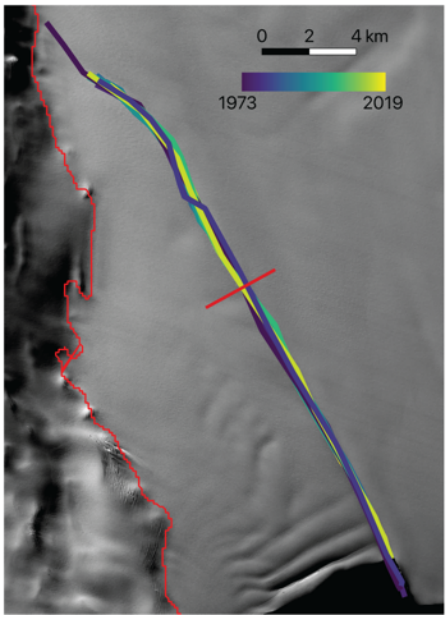

Figure 1c: Digitizations of channels continued

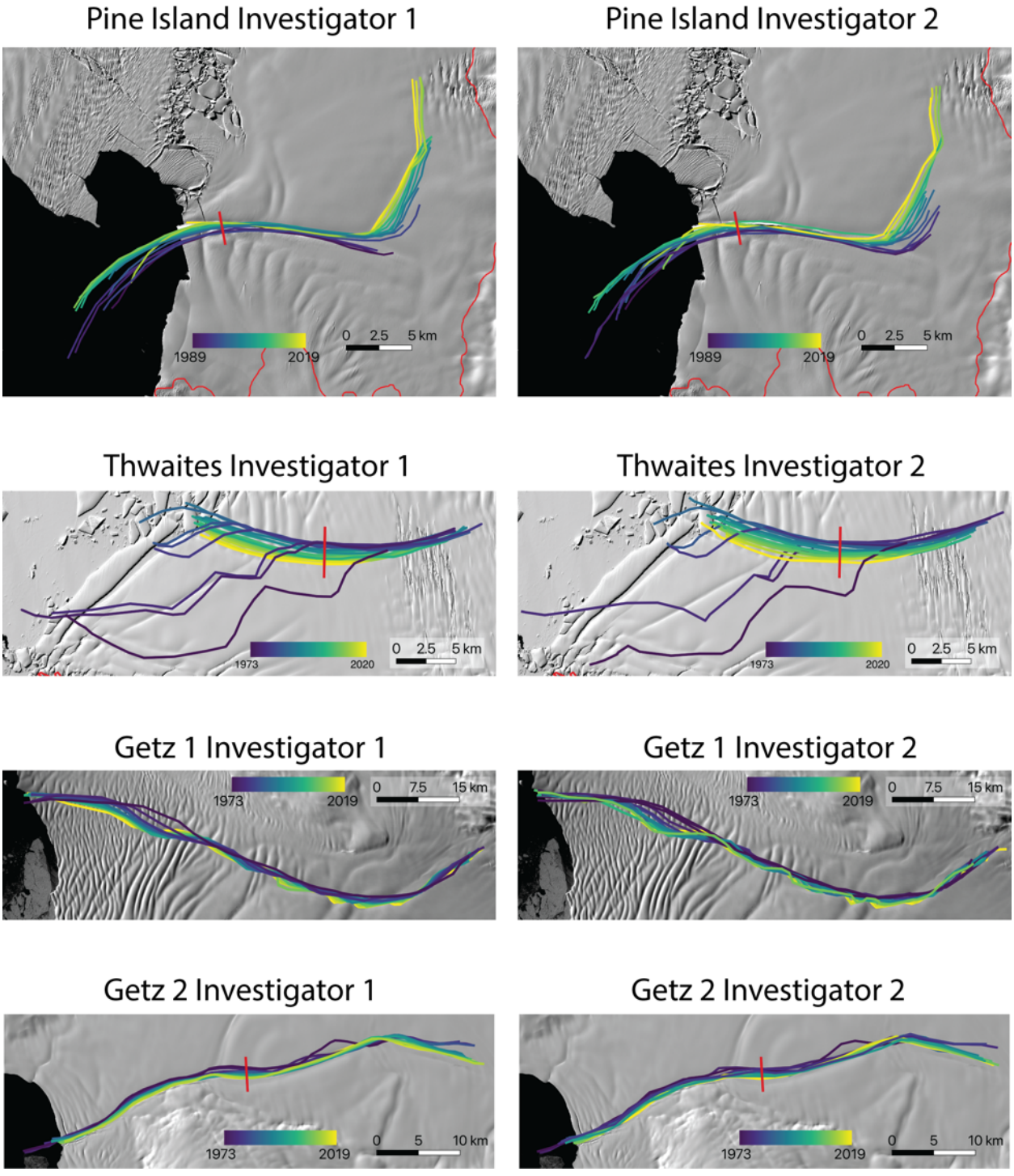

Figure 2a: Channel sinuosity change through time

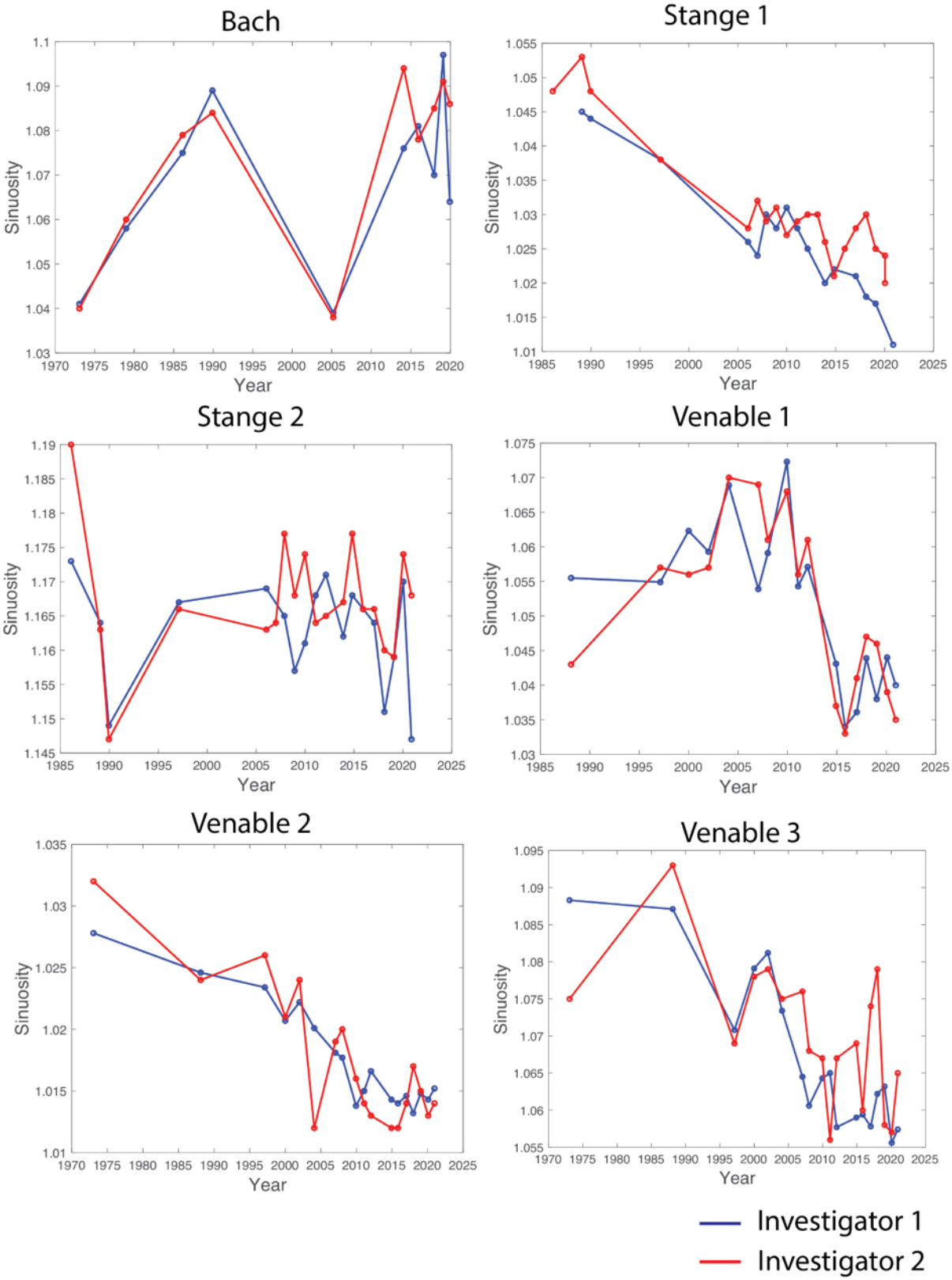

Figure 2b: Channel sinuosity change through time continued

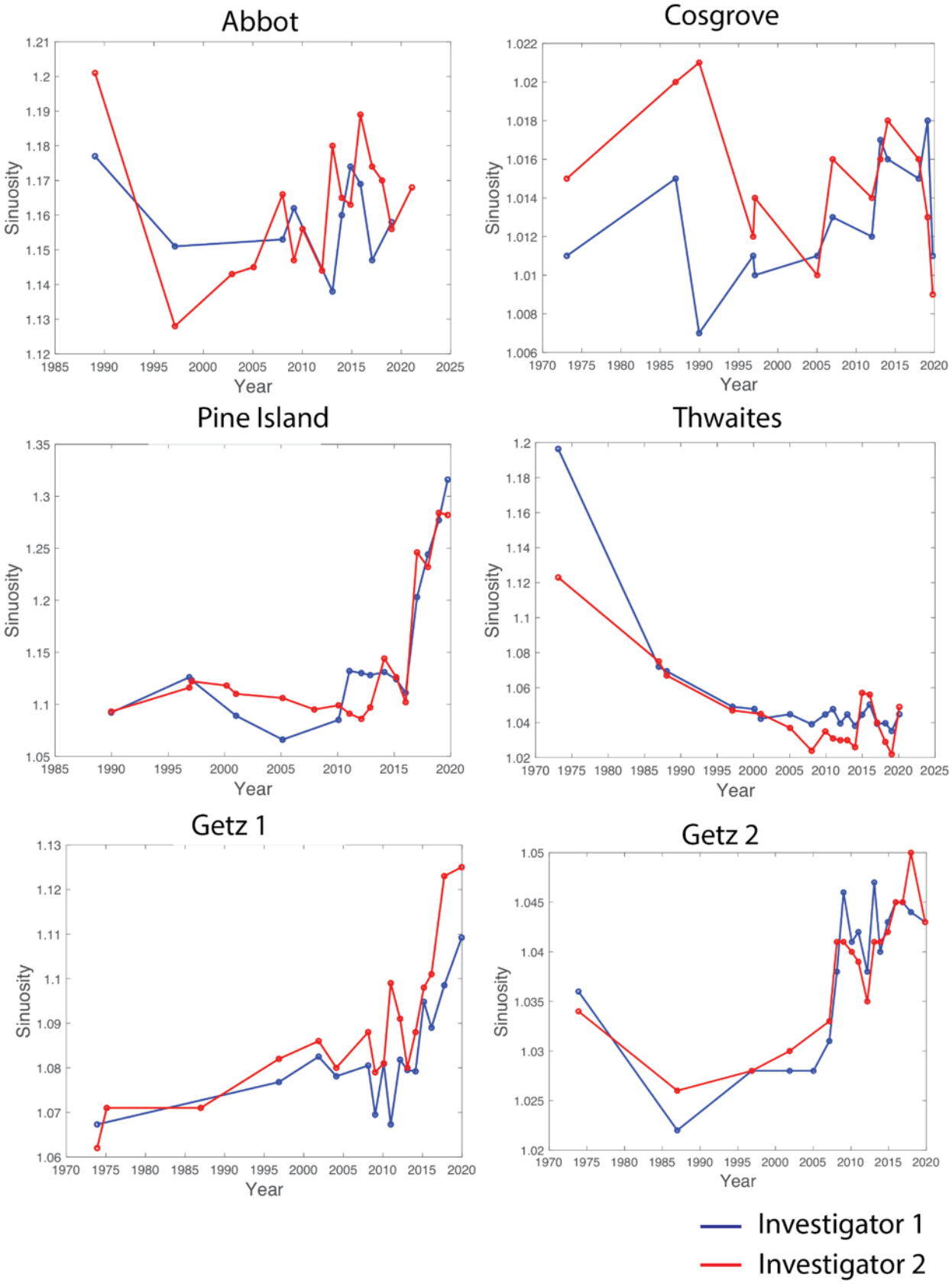

Figure 3: Lateral channel migration based on profiles from Investigator 2

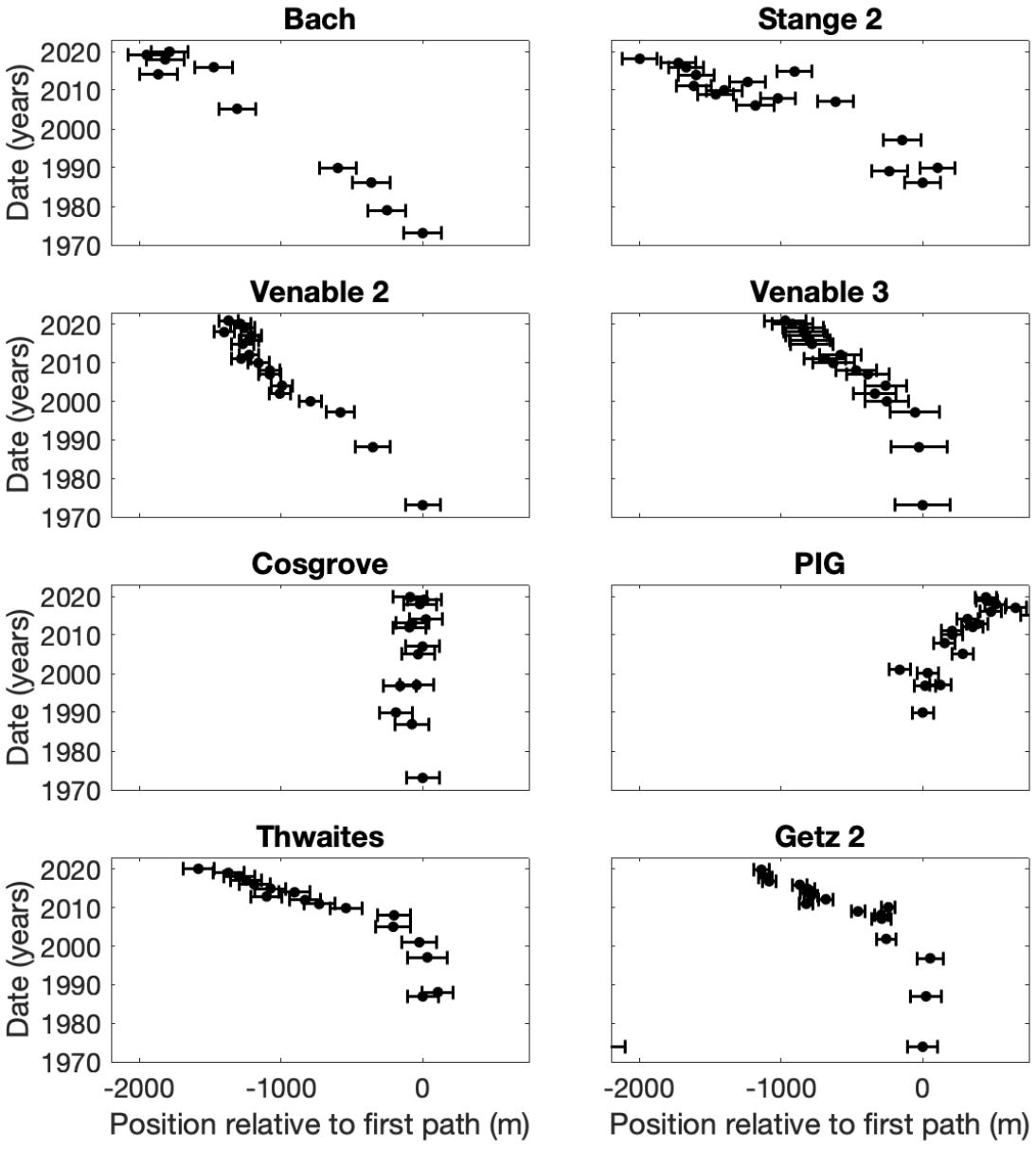

Figure 4a: Channel migrations using MEaSUREs. Original, predicted, and observed positions of channels migrated using the MEaSUREs (Rignot et al. 2016) dataset. The migration of the Thwaites Channel using the Alley et al. (2021) velocity dataset is included in both supplemental figures 3 and 4.

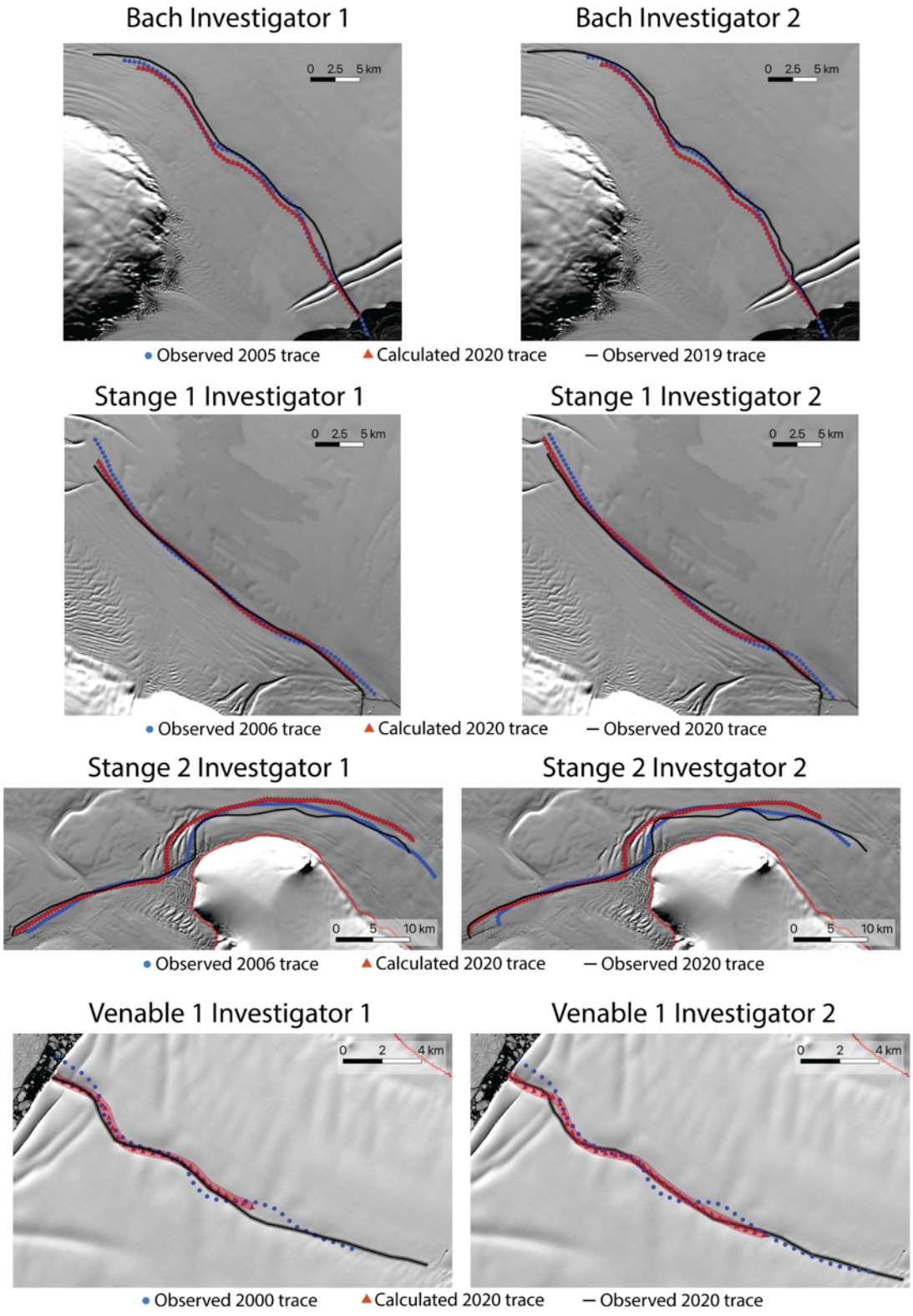

Figure 4b: Channel migrations using MEaSUREs continued.

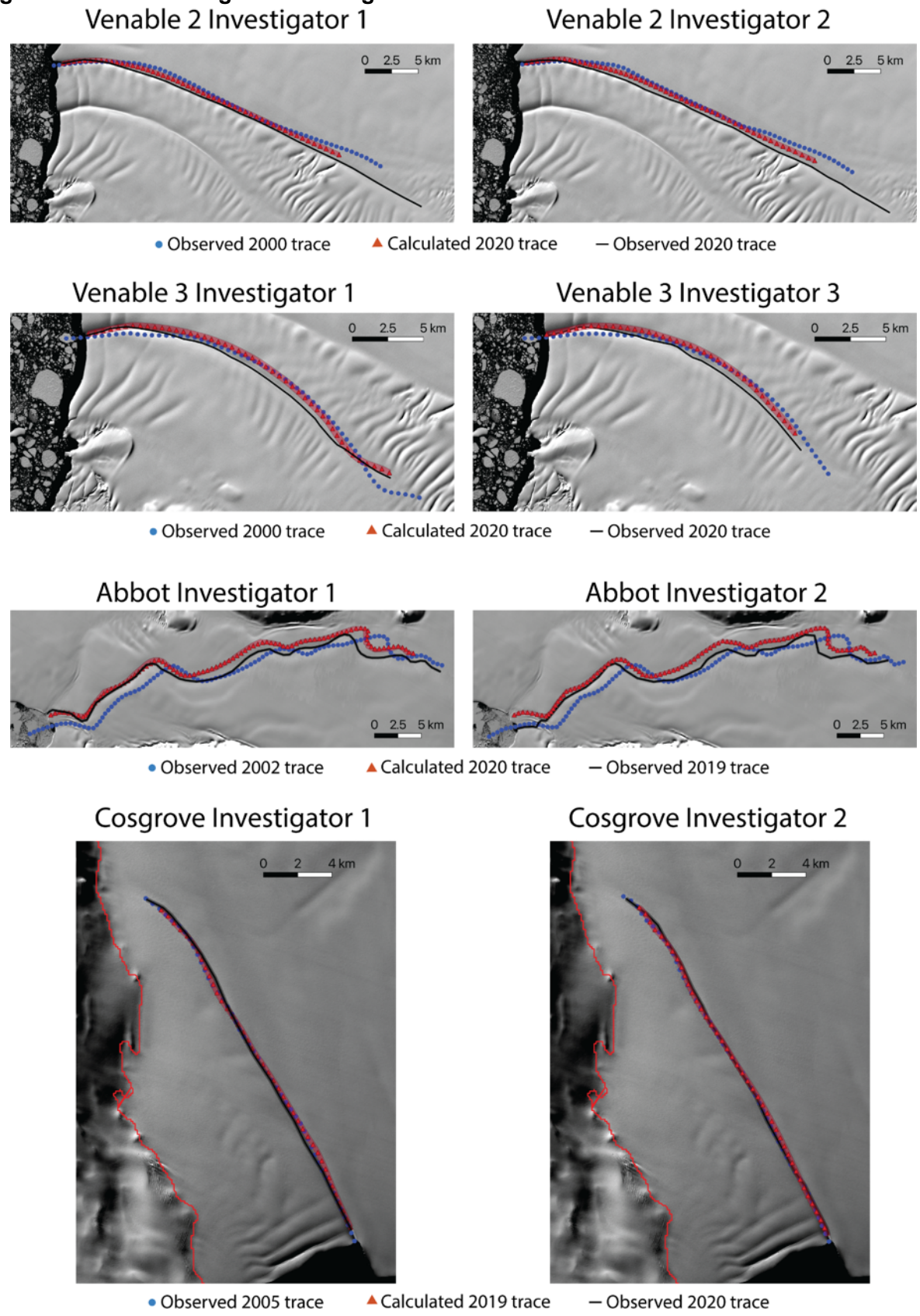

Figure 4c: Channel migrations using MEaSUREs continued

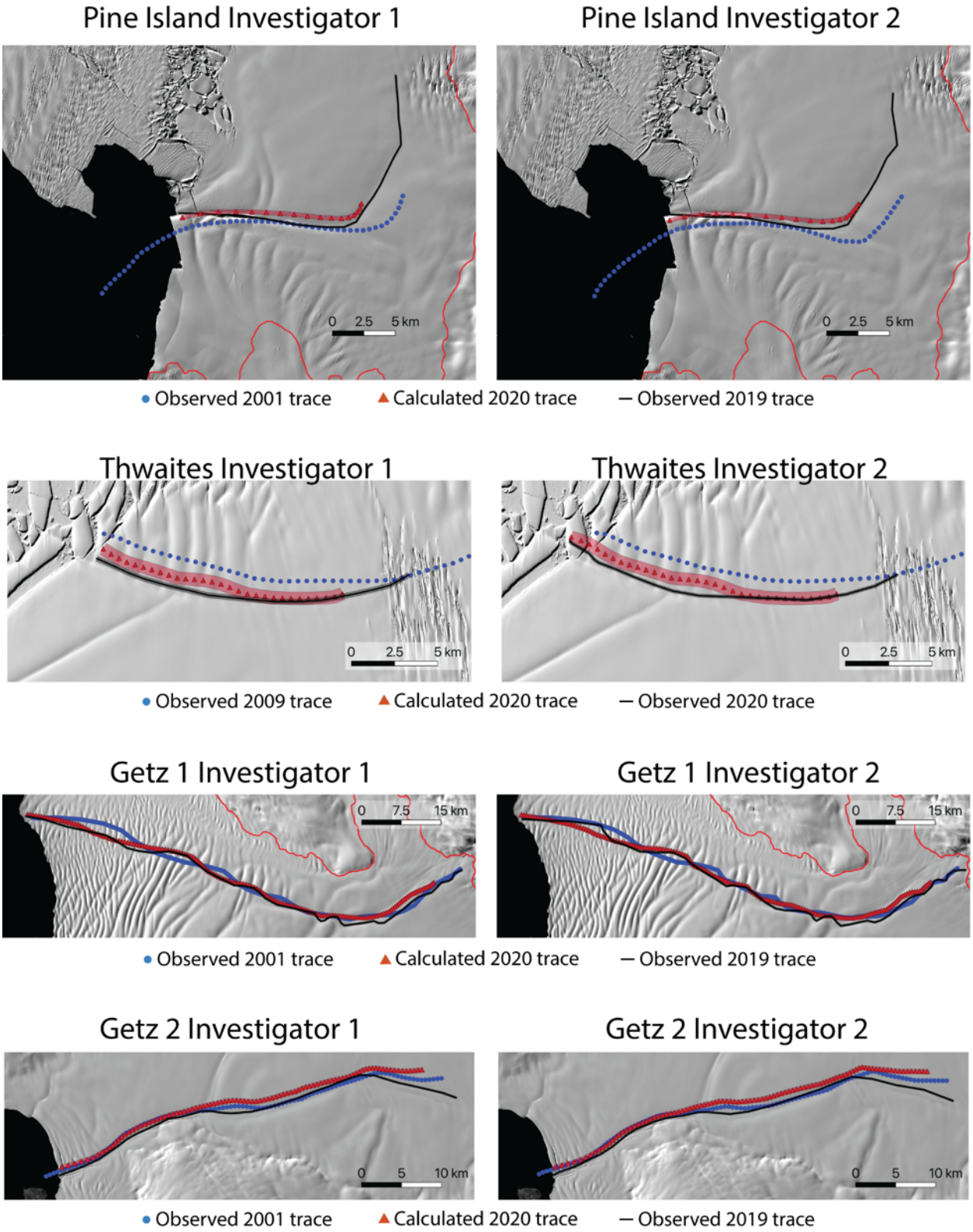

Figure 5a: Channel migrations using ITS_LIVE. Original, predicted, and observed positions of channels migrated using the ITS_LIVE (Gardner et al. 2019) dataset. The migration of the Thwaites Channel using the Alley et al. (2021) velocity dataset is included in both supplemental figures 3 and 4.

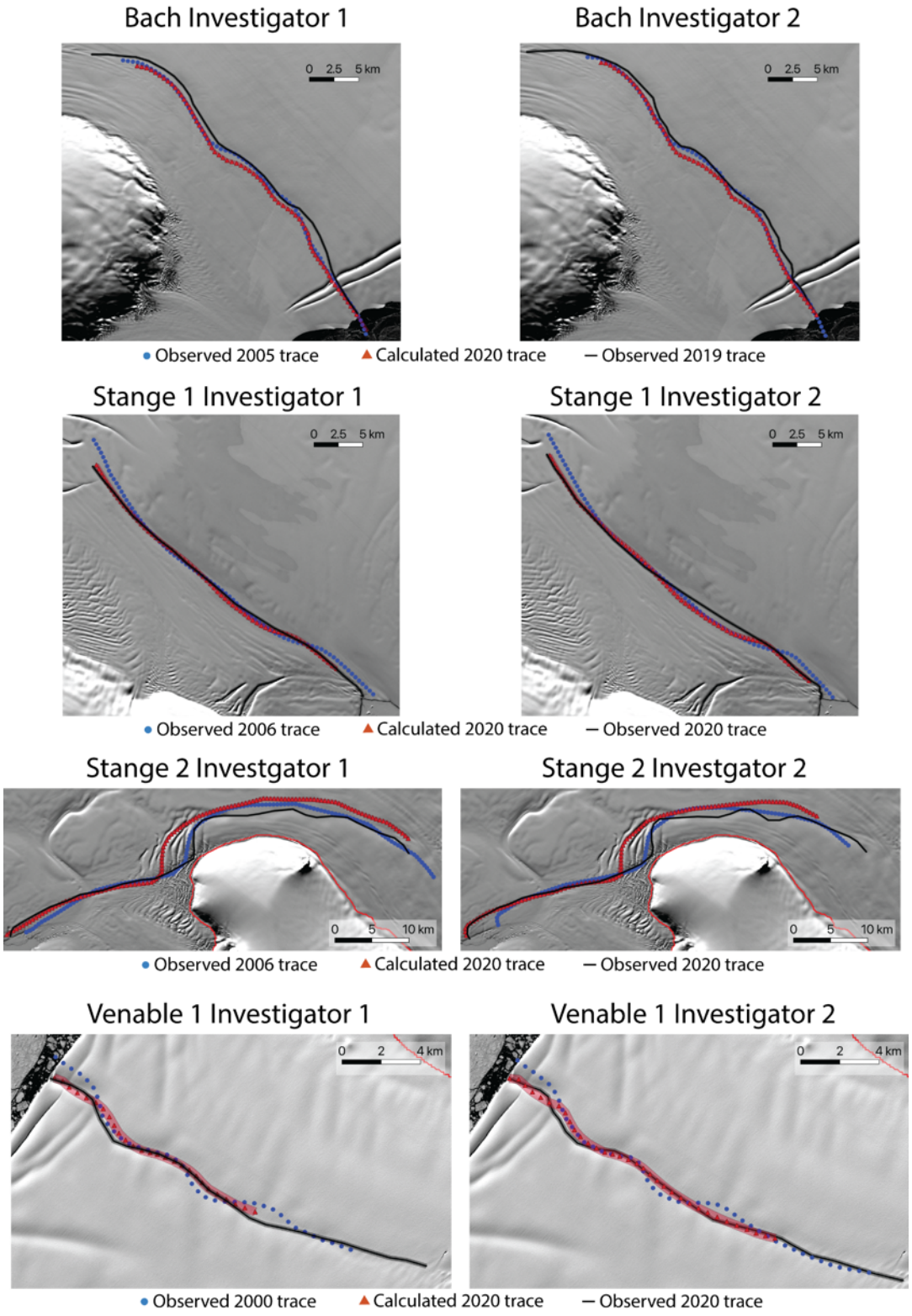

Figure 5b: Channel migrations using ITS_LIVE continued

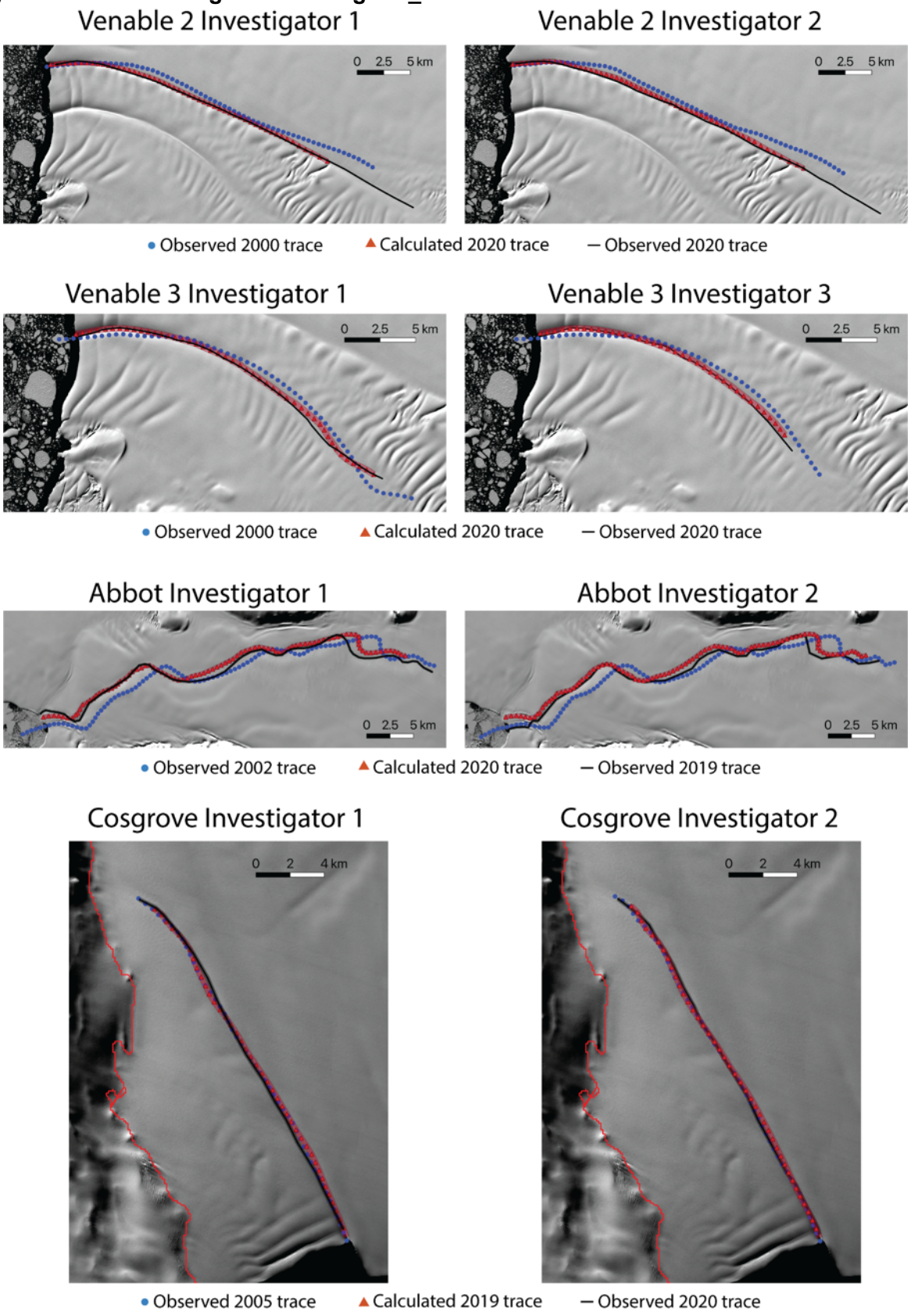

Figure 5c: Channel migrations using ITS_LIVE continued

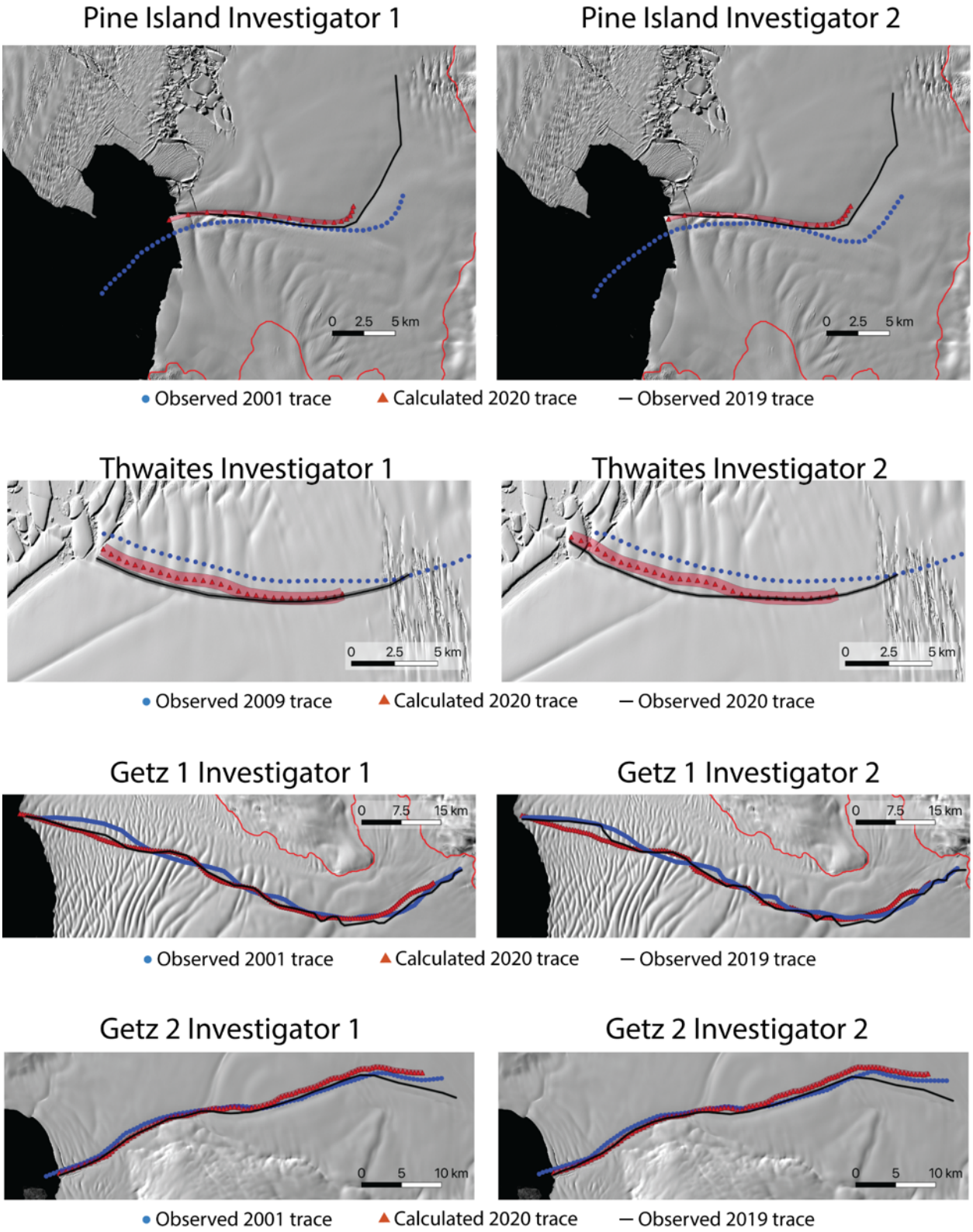

Figure 6: Flow-independent lateral channel migration including both significant and insignificant changes. Colored bars show the percentage of each channel length that migrated to the left or right of its predicted location based on ice flow (Materials and Methods). Columns show the results based on two investigators independently tracing each channel, and rows show results produced with two published velocity fields: MEaSUREs (Rignot et al. 2016) and ITS_LIVE (Gardner 2019).

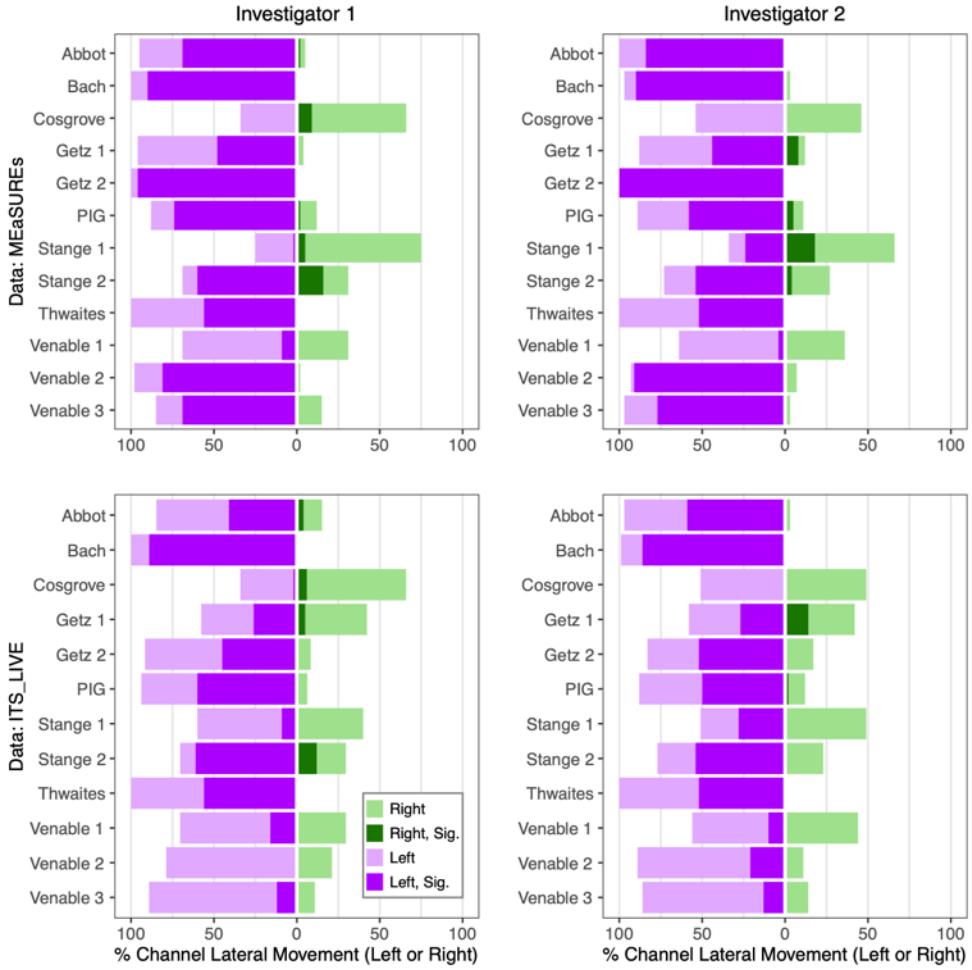

Figure 7: Landsat time-series for Getz 1

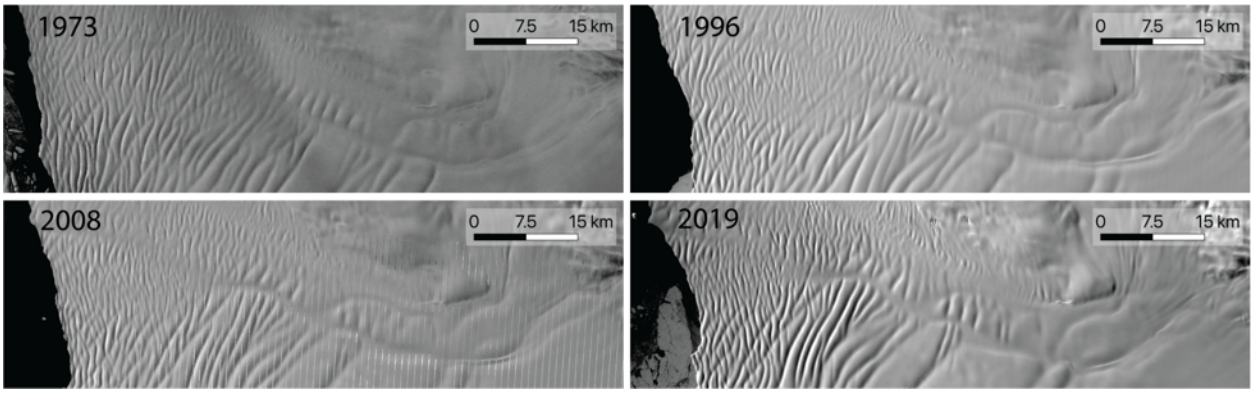

Figure 8: Ground-penetrating radar transects showing leftward channel migration for four example channels. Data from Venable 2, Venable 3, and Thwaites are from IceBridge snow radar, showing only the upper layers of the ice shelf. Data for Abbot are from IceBridge accumulation radar, which penetrates to the base of the ice shelf. White arrow in Abbot radar image shows approximate location of current surface expression of the basal channel. Basal channel locations are in red in inset maps, and ice-shelf surface picks are in pink in radargrams. The surface velocity field in map insets is from MEaSUREs.

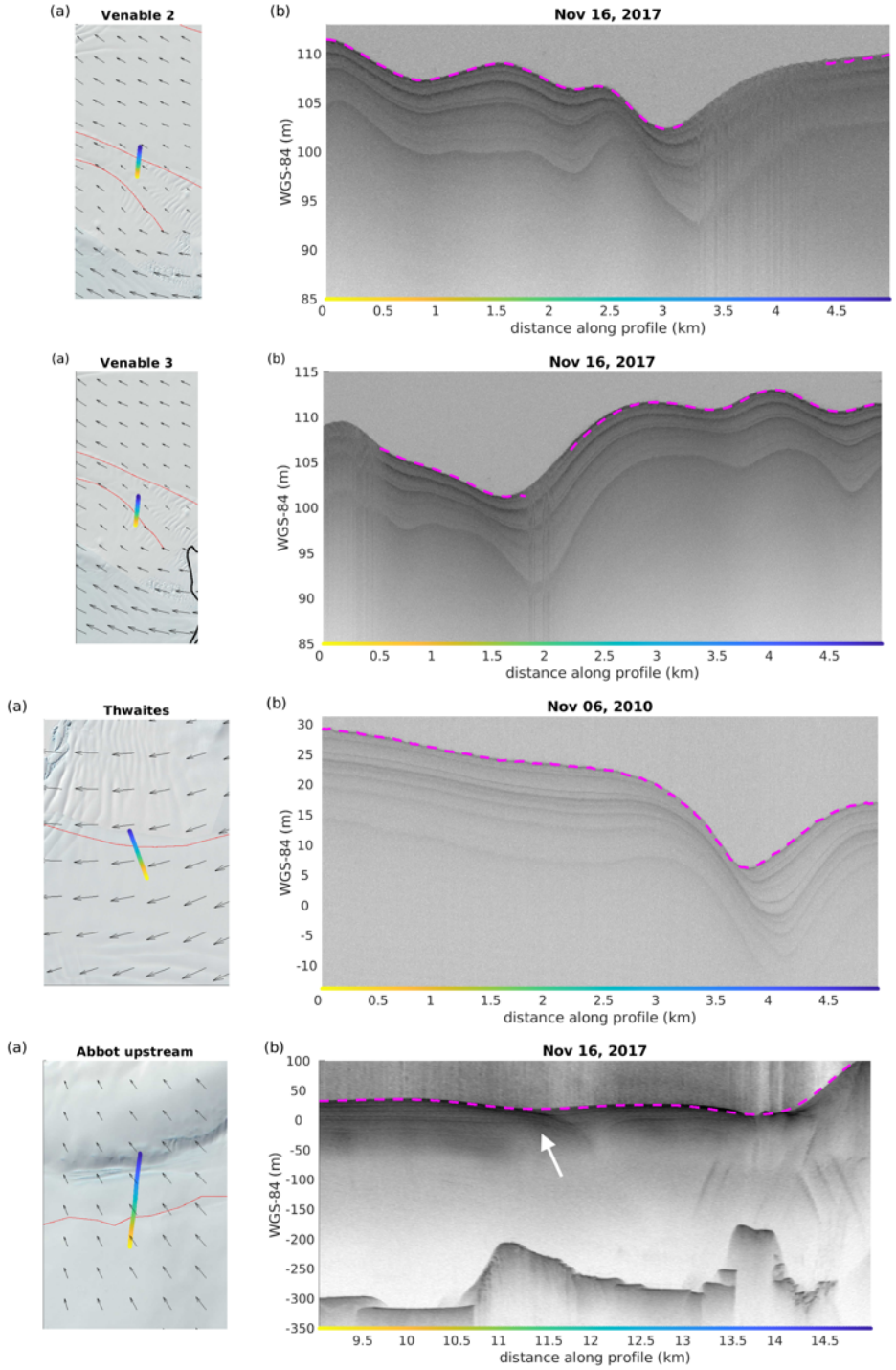

Figure 9: Map of Thwaites air photo flight lines. The orange lines on the map are the flight paths and the blue arrows represent the direction oblique images are facing. The background image is from USGS (1966) and USGS (1967). Air photos are found in supplementary videos as follows:
Supplementary Video 1: Line 5136, collected in 1947
Supplementary Video 2: Same as Supplementary Video 1, but zoomed in on the ice shelf
Supplementary Video 3: Line 1903, collected in 1966
Supplementary Video 4: Line 1989, collected in 1966
Supplementary Video 5: Same as Supplementary Video 4, but zoomed in on the ice shelf
Supplementary Video 6: Line 1991, collected in 1966

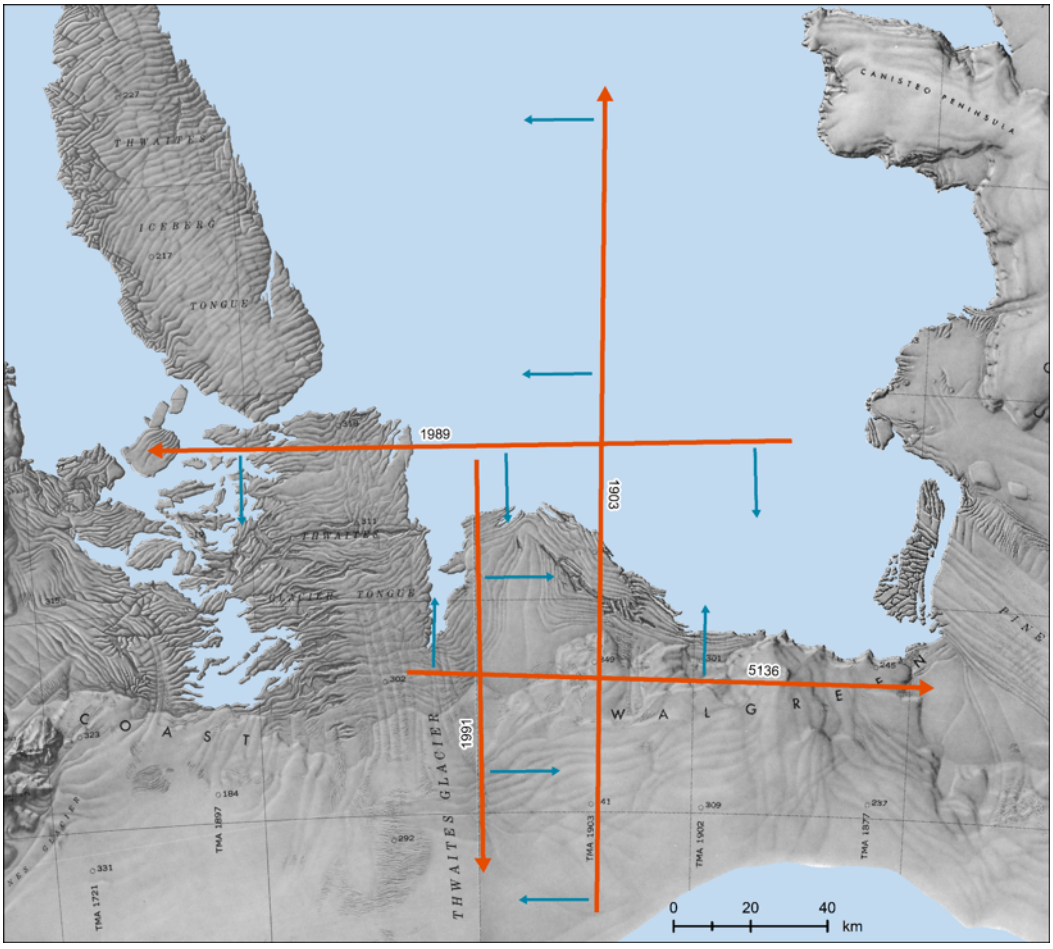

United States Geological Survey (1966). *Antarctica Sketch Map Bakutis Coast - Marie Byrd Land*, 1:500,000. Washington, D.C.: United States Department of the Interior Geological Survey.

United States Geological Survey (1967). *Antarctica Sketch Map Thurston Island - Jones Mountains*, 1:500,000. Washington, D.C.: United States Department of the Interior Geological Survey.

Table 1: Uncertainty calculation for each channel.

Channel	Avg. speed (m/yr)	Avg. ITS_LIVE error (m/yr)	Avg. MEaSUREs error (m/yr)	Max speed trend (m/yr)	Max rotation trend (˚/yr)	Trace error (m)	Total ITS_LIVE error (m)	Total MEaSUREs error (m)
Abbot	133	4.9	3.1	1.4	0.0	131	220	192
Bach	95	3.3	2	0.0	0.0	132	175	158
Cosgrove	94	3	2.1	0.0	0.0	117	162	149
Getz 1	362	3.1	1.88	2.9	0.0	220	302	280
Getz 2	85	5.5	1.6	3.2	2.5	141	335	265
Pine Island	655	1.41	1.8	6.6	0.0	75	160	167
Stange 1	184	3.8	2.9	3.1	0.4	161	252	240
Stange 2	275	3.1	2.3	3.4	0.2	124	205	194
Thwaites	603	26				105	365	
Venable 1	241	5	4.7	0.0	0.0	114	219	213
Venable 2	238	3.7	3.6	0.0	0.9	66	226	224
Venable 3	173	3.8	3.5	1.6	1.3	44	220	214

Supplementary Text 1:

In the main text, we discuss a conceptual model (Figure 9) of steady and non-steady channel paths that is dependent on ice flow and Coriolis-influenced melt. In the following section, we develop analytical solutions for channel path shape under two simple cases, and simple numerical approximations of the steady and non-steady scenarios discussed in the main text.

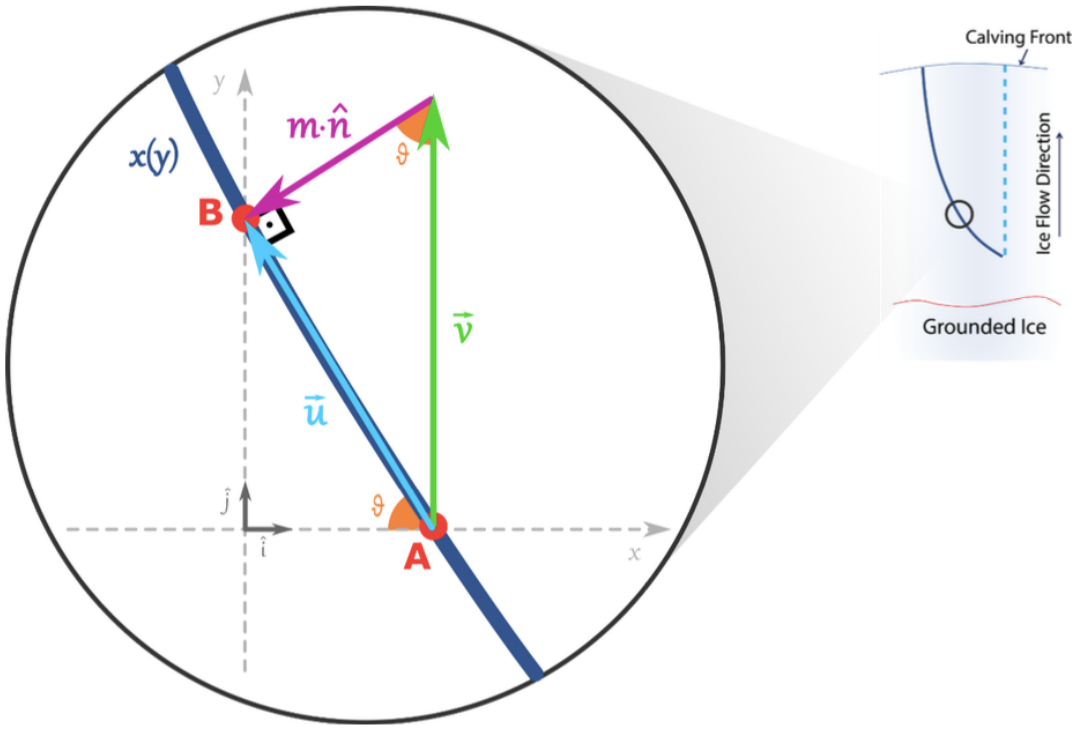

Consider a "channel parcel" moving from point **A** to point **B** with velocity $\vec{u}$. The ice shelf on which the channel is located flows with velocity $\vec{v}$ and the Coriolis-influenced melt happens at a rate m in the direction of the unit vector $\hat{n}$, which is perpendicular to the channel. From the figure above,

$$\vec{u} = \vec{v} + m \cdot \hat{n} \tag{1}$$

If we multiply (1) by $\hat{n}$, we have

$$\vec{u} \cdot \hat{n} = \vec{v} \cdot \hat{n} + m \cdot \hat{n} \cdot \hat{n}$$

or

$$\vec{v} \cdot \hat{n} + m = 0 \tag{2}$$

given that $\vec{u} \perp \hat{n}$ and $\hat{n} \cdot \hat{n} = 1$.

From the figure above, the vectors' components can be written as

$$\vec{u} = -u_x\hat{\imath} + u_y\hat{\jmath}$$

$$\vec{v} = 0\hat{\imath} + v_y\hat{\jmath} \tag{3a-c}$$

$$\hat{n} = -n_x\hat{\imath} - n_y\hat{\jmath}$$

where $\hat{\imath}$ and $\hat{\jmath}$ are unit vectors in the x and y axes, respectively. Substituting (3b) and (3c) into (2):

$$(0\hat{\imath} + v_y\hat{\jmath}) \cdot (-n_x\hat{\imath} - n_y\hat{\jmath}) + m = 0$$

$$-v_y n_y + m = 0$$

$$\boxed{n_y = \frac{m}{v_y}} \tag{4}$$

Given that $n^2 = 1 = {n_x}^2 + {n_y}^2$, we have

$${n_x}^2 = 1 - \left(\frac{m}{v_y}\right)^2$$

$$\boxed{n_x = \sqrt{1 - \left(\frac{m}{v_y}\right)^2}} \tag{5}$$

By the similar triangle theorem,

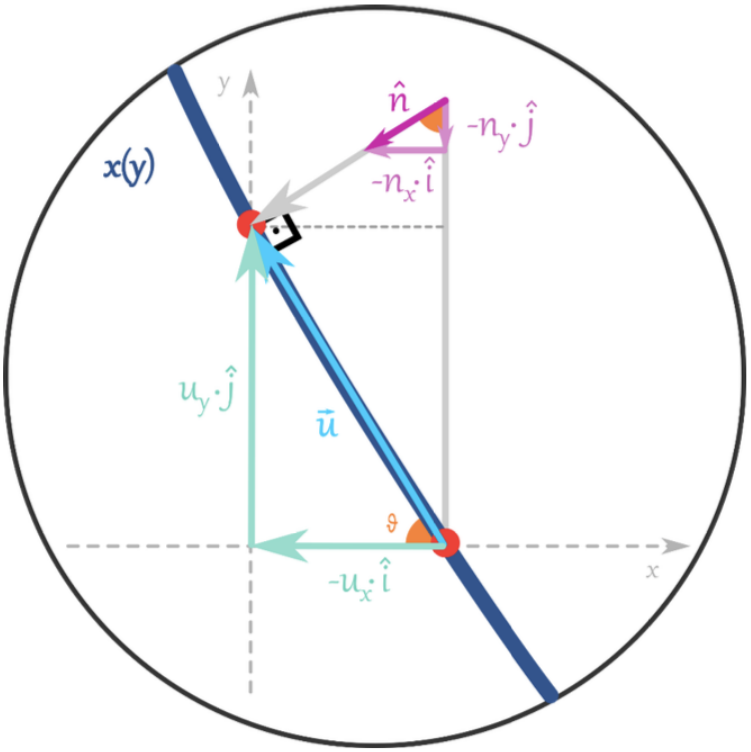

$$\frac{-u_x\hat{\imath}}{u_y\hat{\jmath}} = \frac{-n_y\hat{\jmath}}{-n_x\hat{\imath}}$$

or

$$-u_x n_x = u_y n_y \tag{6}$$

Since $u_x = \frac{dx}{dt}$ and $u_y = \frac{dy}{dt}$, and using (4) and (5), (6) becomes

$$-\sqrt{1 - \left(\frac{m}{v_y}\right)^2}\,\frac{dx}{dt} = \frac{m}{v_y}\frac{dy}{dt}$$

$$\frac{\frac{dx}{dt}}{\frac{dy}{dt}} = -\frac{\frac{m}{v_y}}{\sqrt{1-\left(\frac{m}{v_y}\right)^2}}$$

$$\boxed{\frac{dx}{dy} = -\frac{\frac{m}{v_y}}{\sqrt{1-\left(\frac{m}{v_y}\right)^2}}} \quad (7)$$

To find the shape of the channel, $x(y)$, we need to solve (7). It is possible to solve it analytically for simple cases, such as

(a) when m and v_y are constant:

$$\int \frac{dx}{dy}dy = \int -\frac{\frac{m}{v_y}}{\sqrt{1-\left(\frac{m}{v_y}\right)^2}}dy$$

$$\int dx = -\frac{\frac{m}{v_y}}{\sqrt{1-\left(\frac{m}{v_y}\right)^2}}\int dy$$

$$x(y) = -\frac{\frac{m}{v_y}}{\sqrt{1-\left(\frac{m}{v_y}\right)^2}}y \quad (8)$$

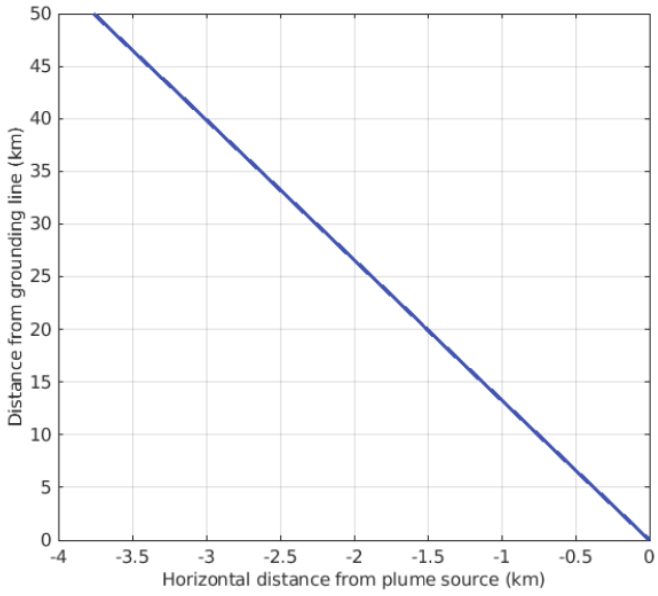

(b) when m is constant but v_y varies linearly along y, i.e.,

$$v_y = v_0 + ay \quad (9)$$

and

$$dv_y = a.dy \quad (10)$$

where a is a strain rate. We then have

$$\int \frac{dx}{dy}dy = \int -\frac{\frac{m}{v_y}}{\sqrt{1-\left(\frac{m}{v_y}\right)^2}}dy$$

$$\int dx = -\int \frac{m}{v_y \sqrt{1 - \frac{m^2}{{v_y}^2}}} dy \tag{11}$$

Multiplying the right hand side of (11) by a/a and substituting $a.dy$ by dv_y according to (10),

$$x(v_y) = -\frac{1}{a}\int \frac{m\, dv_y}{\sqrt{{v_y}^2 - m^2}}$$

$$x(v_y) = -\frac{m}{a}\ln\left|v_y + \sqrt{{v_y}^2 - m^2}\right|$$

or, using (9),

$$x(y) = -\frac{m}{a}\ln\left|v_0 + ay + \sqrt{(v_0 + ay)^2 - m^2}\right| \tag{12}$$

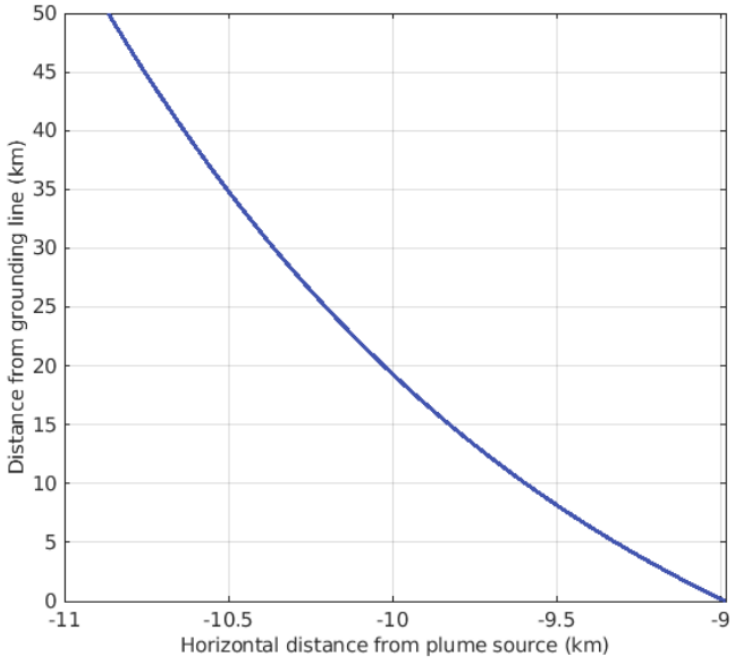

We have also calculated $x(y)$ numerically, by assuming $\frac{dx}{dy} \to \frac{\Delta x}{\Delta y}$ when $dy \to 0$. In this case, (7) becomes

$$x_k = x_{k-1} - \left.\frac{\frac{m}{v_y}}{\sqrt{1 - \left(\frac{m}{v_y}\right)^2}}\right|_k (y_k - y_{k-1}) \tag{8}$$

where k is the grid point index in the y direction. Assuming a v increasing linearly along y, and m decreasing linearly along y ,

$$v_y = v_0 + ay$$

$$m = m_0 - by$$

and using typical values/orders of magnitude for ice shelf flow, strain rate, and melt rates:

	AVERAGE	DECREASED	INCREASED
$v_0\ (m/yr)$	200	100	400
$m_0\ (m/yr)$	15	7.5	30
$a\ (yr^{-1})$	10^{-3}	-	-
$b\ (yr^{-1})$	10^{-7}	-	-

we have results similar to the schematic in Figure 9c-f: